Field-emission scanning electron microscopy of cochlear hair cells: tip links, lateral links and tip junctions on stereocilia

C.M. Hackney and D.N. Furness

Department of Communication & Neuroscience, Keele University, Keele, Staffordshire ST5 5BG

It has been proposed that the mechanotransduction channels in all vertebrate hair cells are gated by tip links which run between the tips of the shorter stereocilia and the sides of the stereocilia in the next row (see e.g., Pickles & Corey, 1992). However, recent attempts to localize the channels immunocytochemically suggest that they may be positioned at a junction-like structure that has been observed, using transmission electron microscopy, at the point where the stereocilia of adjacent rows come into closest contact with each other. The tip junction is thought to be distinct from lateral links which connect the shafts of adjacent stereocilia (Hackney *et al.* 1992).

The relative positions and morphology of tip links, lateral links and tip junctions will be demonstrated using field emission scanning electron microscopy (FESEM) in which high resolution (better than 2 nm) can be obtained at low accelerating voltages, e.g. 5 kV. This enables examination of stereociliary bundles that have less coating than is generally required for conventional scanning electron microscopy, thus permitting the observation of finer surface detail.

To obtain these specimens, guinea-pigs (250–600 g) were killed by giving an overdose of sodium pentobarbitone (400 mg kg^{-1} I.P.), decapitated and the bullae opened. Red-eared terrapins (*Trachemys scripta elegans*) with carapaces 8–9 cm in length were anaesthetized with ketamine (160 mg kg^{-1}), decapitated and the cochlear duct dissected out in artificial perilymph of composition (mM): 130 NaCl, 4 KCl, 2·2 $MgCl_2$, 2·8 $CaCl_2$, 5 Na-Hepes, pH 7·6. It was then exposed for 20 min to subtilisin BPN′ (30 $\mu g\ ml^{-1}$, Sigma) made up in the same solution, and the tectorial membrane peeled from the underlying epithelium. For fixation both mammalian and reptilian cochleas were perfused with 2·5% glutaraldehyde in 0·1 M sodium cacodylate buffer (pH 7·4) containing 2 mM $CaCl_2$, then washed in the same buffer and post-fixed for 1 h in 1% osmium tetroxide. They were then impregnated with further osmium by immersing them 2–3 times for 1 h in 1% OsO_4 alternating with 20 min in a saturated solution of sodium thiocarbohydrazide interspersed by thorough washing in distilled water, prior to dehydration via an ethanol series and critical point-drying using carbon dioxide as the transitional fluid.

With FESEM, tip links can be seen to divide into two or more strands at the point at which they are attached to the sides of the tall stereocilia. Lateral links occur as arrays of filaments with a thickened central region between the shafts of the stereocilia. The tip junction is distinct in position and morphology from the lateral linkages, often appearing as a closely apposed area of membrane between the tips and sides of adjacent short and tall stereocilia.

Deflections of the bundle would cause shearing at the tip junction if sliding can occur here, possibly opening the mechanotransduction channels if they are indeed located at this point. The tip and lateral links may be to ensure that the bundle moves as a whole if it is deflected and may also maintain the stereocilia in close contact with each other at the tip junction. The tip links are also well situated to act as a means, in addition to the stiffness provided by actin filaments in the stereocilia themselves, of returning the stereocilia to their resting position following deflections in the direction of the tallest row.

Supported by the Wellcome Trust and Hearing Research Trust.

REFERENCES

Hackney, C.M., Furness, D.N., Benos, D.J., Woodley, J.F. & Barratt, J. (1992). *Proc. R. Soc.* B **248**, 215–221.
Pickles, J.O. & Corey, D.P. (1992). *TINS* **15**, 254–259.

A computational model of the cochlea and cochlear nerve for teaching and research

E.F. Evans

Department of Communication & Neuroscience, Keele University, Keele, Staffordshire ST5 5BG

Since 1974, we have had in routine use in the laboratory, a hardware analogue of the cochlea and cochlear nerve (Evans, 1979, 1980). This simulates, in real-time, the salient features of the mammalian single cochlear nerve fibre discharges. It has proved valuable for three reasons. Firstly, it has allowed rehearsal and optimization of manual and computer-controlled strategies of response analyses, particularly automated threshold and receptive field mapping (e.g. Evans, 1979; Evans *et al.* 1987). Secondly, it has proved valuable for teaching purposes, enabling students to have 'hands-on' experience of determining thresholds, receptive fields and rate-level functions, phase-locking and other suprathreshold properties of cochlear nerve fibres. Thirdly, it, and its software successor, is allowing a systematic investigation of the importance of certain features of the model in determining the matching of its performance to the responses of mammalian nerve fibres to a wide range of complex stimuli (e.g. Evans, 1987, 1988, 1989).

Unlike the hardware model, this version can be run in its entirety on a PC, complete with the generation of signal inputs and visual and auditory output. The computational model takes the above hardware model as its basis. It is constructed in LabVIEW (National Instruments UK Corp., 21 Kingfisher Court, Hambridge Road, Newbury, Berks RG14 5SJ) and can run somewhat faster than real-time on a 66 MHz 486DX PC. It accepts stimuli selected by mouse or keyboard from a repertoire of previously synthesized stimuli or generated in

real-time as directed by 'controls' displayed on the monitor and manipulated by mouse or keyboard. It generates an oscilloscope-like view of the output action potentials in time, audible as clicks over the PC's loudspeaker or sound card. For research purposes, the parameters of the model can be easily manipulated via an array of 'front-panel controls' on the display, and the responses of any stage of the model visualized by an oscilloscope-like display, or written to file. It reproduces over a wide range of stimulus levels (100 dB) the following characteristics: suprathreshold tuning properties to tones and noise, discharge rates, intensity functions, post-stimulus time, period and inter-spike interval histograms, autocorrelograms in response to tones, noise, clicks and multi-component stimuli and reverse correlograms to noise.

LabVIEW has the singular advantages that the model's development, modification, testing and display of output can be accomplished very rapidly without writing any text code, by the graphical 'wiring up' on screen of iconized functions from a very large function library. New functions can be built up from the existing functions and/or from purpose-built functions constructed from simple formulae or 'C' code. Conventional programming facilities such as file and array handling, while- and for-loops, case, and sequence structures, etc., are easily incorporated. A stand-alone, compiled version of the model can be generated for tamper-free class use.

Physiological justification for the stages of the model is summarized in Evans (1975). Briefly, a front-end bandpass filter filters the incoming signal by convolution with a chosen impulse response (gammatone or reverse correlogram taken from our physiological data). An AGC limiter simulates saturation of the mean discharge rate without corrupting the period histogram of stimuli at levels above saturation. A halfwave rectifier simulates unidirectional excitation at the hair cell level. A logarithmic compression stage simulates the relation between spike rate and stimulus amplitude between threshold and saturation. High pass filtering provides adaptation and off-suppression. Probabilistic spike generation is simulated by two-quadrant multiplication between the processed signal and noise followed by level detection, so that the probability of discharge is related to the halfwave rectified stimulus waveform. An absolute refractory period of 2 ms follows each spike.

Supported by the EPSRC.

REFERENCES

Evans, E.F. (1975). In *Handbook of Sensory Physiology*, vol. V/2: Auditory System, ed. Keidel, W.D. & Neff, W.D., pp. 1–108. Springer-Verlag, Heidelberg.

Evans, E.F. (1979). In *Auditory Investigations: The Scientific and Technological Basis*, ed. Beagley, H.A., pp. 324–367. Oxford University Press, Oxford.

Evans, E.F. (1980). *J. Physiol.* **298**, 6–7*P*.

Evans, E.F. (1987). *Br. J. Audiol.* **21**, 311.

Evans, E.F., Cooper, N.P. & Birch, J.L. (1987). *Br. J. Audiol.* **21**, 318.

Evans, E.F. (1988). *Br. J. Audiol.* **22**, 136.

Evans, E.F. (1989). In *Cochlear Mechanisms – Structure Function and Models*, ed. Wilson, J.P. & Kemp, D.T., pp. 241–250. Plenum Publishing Corporation, NY, USA.

Apparatus and software for delivering waveforms of drug concentrations using pulse width modulation

P. Kumar, D.A. Davies, J. Nally and D.R. Pepper

Department of Physiology, Medical School, University of Birmingham, Birmingham B15 2TT

We will demonstrate a method that we have used to present repeated, reproducible waveforms and steady levels in the concentration of drugs and ions and/or dissolved gas tensions to a superfused *in vitro* carotid body preparation. The method is, however, also suitable for any system that requires the application of a number of different drug concentrations to a preparation from which, for example, a dose–response curve can be generated. Most often this is performed by sequential application of serially diluted concentrations of an accurately prepared stock solution. A disadvantage of this approach is the potential for inaccuracies to occur with each dilution and also with the limitation to steady-state application of a relatively small number of different concentrations.

Two prepared solutions are delivered by a peristaltic pump to the two input ports of an electronic pinch valve (Cole-Parmer), one tube of which is normally open and the other normally closed. The two output ports are connected by a Y-piece and this single, admixture output passed, via a small volume mixing chamber, to the preparation. The duty cycle of a 1 Hz, 12 V DC square wave controlling the pinch valve is varied by pulse-width modulation using a voltage comparison between a 1 Hz, $\pm$ 5 V triangle-wave generator (composed of an integrator and comparator) and a $\pm$ 5 V waveform-generating routine written using the LabVIEW programming environment (National Instruments) and running on a Macintosh IIci microcomputer equipped with a National Instruments NB-MIO-16H A/D data aquisition board. In this way, concentrations lying between those of the two prepared solutions, usually a zero-drug control level and the highest concentration of drug required, can be produced by generation of the appropriate sequence of duty cycles. The system is also designed to run, at lower cost, without a microcomputer, to produce steady concentration levels, between those of the two prepared solutions, by means of a voltage comparison between the triangle-wave generator and a steady voltage level set by a push button potentiometer. We will demonstrate a variety of forcing functions imposed upon acid concentration as measured by a commercial pH meter and will also show data previously collected in our laboratory demonstrating the effect of varying extracellular $[K^+]$ upon chemoreceptor discharge and which also shows the potential of this system for generating response curves on-line.

We acknowledge the support of the MRC and the Wellcome Trust.

Using a PC sound card to record otoacoustic emission data

Paul J. Kolston, Lara F. Gee and Katharine S. Tomlins

Department of Physiology, University of Bristol, Bristol BS8 1TD

Sound cards are widely used in consumer and business multimedia environments, making them affordable in a variety of applications. Occupying a standard AT-expansion slot of an IBM-compatible personal computer, they provide two input/output channels with a sampling or playback rate of 44 kHz at true 16-bit resolution. These samples are stored directly to the hard disk in real time, making very long sampling periods possible. The specifications of these sound cards makes them suitable for the acquisition of physiological data.

Here we demonstrate a system using a Sound Blaster® (Creative Labs) sound card to record spontaneous otoacoustic emissions in human subjects. Virtually all mammalian ears emit these sounds, either spontaneously or following ipsilateral sound stimulation. Otoacoustic emissions (OAEs) are generated within the cochlea and provide invaluable insight into cochlear integrity (Probst *et al.* 1991). We have designed an otoacoustic probe incorporating both microphone and power supply. This is placed in the ear canal and ear muffs are used to attenuate environmental noise during recording. The sound card captures the data, which are subsequently processed using a standard data analysis package. The frequency spectra of several samples are obtained using a fast Fourier transform algorithm, before being averaged to extract the emission signals from the background noise. Using this method it is evident that the emissions consist of narrow-band peaks concentrated in the frequency range of normal speech.

There is considerable evidence that the generation of OAEs is related to normal cochlear tuning, but the nature of the underlying mechanisms is still unclear. Spontaneous OAEs provide direct evidence of an energy-generating process within the cochlea, presumably reflecting that outer hair cell force generation observed in isolated cells *in vitro* also occurs *in vivo*. We will demonstrate how stimulation of the contralateral ear alters the emission frequencies, presumably either through a descending fibre tract from the superior olivary complex known as the olivocochlear bundle, or via the middle ear acoustic reflex (Harrison & Burns, 1993).

REFERENCES

Harrison, W.A. & Burns, E.M. (1993). *J. Acoust. Soc. Am.* **94**, 2649–2658.

Probst, R., Lonsbury-Martin, B.L. & Martin, G.K. (1991). *J. Acoust. Soc. Am.* **89**, 2027–2067.

Entoptic visualization of macular pigment

Jack D. Moreland

Department of Communication & Neuroscience, Keele University, Keele, Staffordshire ST5 5BG

Macular pigment is found in primate retinae and is concentrated in the region of the fovea forming the ophthalmologically visible 'yellow spot'. This pigment (a mix of two carotenoids: Zeaxanthin and Lutein with similar absorbance spectra peaking at 462 and 458 nm respectively) forms a screen between incident radiation and the photoreceptors, supplementing the spatially uniform absorption of the lens at short wavelengths. Its presumed functions are: (a) a reduction of the effects of chromatic aberration on visual resolution at the fovea, and (b) protection of the retina from phototoxic damage, first by selective absorption of shortwave radiation and second by quenching active photochemical products such as singlet oxygen and oxygen radicals.

Macular pigment is distributed approximately exponentially around the fovea: decadic angles range from 2 to 5 deg (Moreland & Bhatt, 1984). The peak concentration varies some 10-fold between individuals and, apart from posing problems for the aforementioned hypotheses, significantly affects colour matching and colour vision testing (Moreland & Dain, 1992).

Some macular pigment is bound to the radial receptor axons in Henle's layer and interacts with polarized light generating the Haidinger's brush phenomenon. If blue light is viewed through a rotating polarizer a small dark patch is seen, shaped like a spindle rotating about the fixation point. Since only 10% of macular pigment is oriented systematically, some subjects have difficulty in seeing the effect. However, colour matches are affected by the full complement of pigment in front of the photoreceptors, providing the basis for a more striking demonstration.

In the demonstration, a large bipartite field (14 deg square) is presented. The two half-fields are approximately matched in colour: the appearance being a near-white. The mixtures are cyan and reddish-orange (490 + 610 nm) on the left, and blue and yellowish-green (460 + 570 nm) on the right.

Macular pigment absorbs cyan and blue preferentially and changes the two mixtures reaching the photoreceptors in accordance with its retinal distribution. An observer sees his or her macular pigment projected entoptically as a coloured patch (Maxwell's spot). The patch is about 3 or 4 deg in diameter and changes from 'pink on green' (left) to 'green on pink' (right) on switching gaze between the two half-fields.

Continued gazing reduces the visibility of Maxwell's spot, due to local adaptation (the macular pigment shadow is a 'stabilized image'). Switching gaze between the two half-fields interrupts that by reversing the colour contrast and thereby facilitates visual inspection of the area of highest

pigment concentration. Maxwell's spot is usually somewhat irregular and fine structure may be discerned with careful observation. The effect is similar in both eyes, presumably because the amounts of macular pigment in each are highly correlated.

REFERENCES

Moreland, J.D. & Bhatt, P. (1984). *Documenta Ophthalmologica Proceedings Series* **39**, 127–132.
Moreland, J.D. & Dain, S.L. (1992). *Perception* **21**, 74.

A modified portable fibre optics apparatus for measurements of spectral sensitivity

D. Carden*, I.J. Murray*, N.R.A. Parry† and J.J. Kulikowski*

**Visual Sciences Laboratory, UMIST, Manchester M60 1QD and † Vision Science Centre, Manchester Royal Eye Hospital, Manchester M13 9WH*

Spectral spots larger than 0·6 deg are detected mostly by chromatic opponent mechanisms when presented infrequently (e.g. at 1 Hz) on a photopic white background, 1000 Td (King-Smith & Carden, 1976). Such measurements are usually performed using a Maxwellian view apparatus, which is not portable. We show that a free viewing system using fibre optics, can also be used to reveal chromatic mechanisms. The main developments compared with the Maxwellian view method are directed towards (1) higher degrees of isolation of chromatic-opponent mechanisms, and (2) more flexible balance between the different component chromatic mechanisms. Near detection threshold only four colours are discriminated: red, yellow, green and blue. The electrophysiological evidence points to the correlation of these psychophysical mechanisms with red/green, green/red, blue/yellow and yellow/blue opponent sets of cells in the visual cortex of primates. Among these mechanisms, yellow/blue opponency is the most difficult to demonstrate since achromatic detection is usually more sensitive in the yellow region. Provided colour temperature is optimized (to around 2500 K) an optimum balance between blue and yellow detection mechanisms can be achieved. The system has three notable features:

(1) design based on fibre optics,

(2) a pedestal background, co-extensive with the test spot (Foster & Snelgar, 1983) and adjustable in colour temperature using different filters, and

(3) a dark annulus surround (Kulikowski & Walsh, 1991).

The main advantages of the system are as follows: portability, ease of use, optimization of balance between colour opponent mechanisms, stability of calibration and binocular viewing.

The system has been used under clinical conditions and the modification described here, which allows the manipulation of colour temperature of the coincident field, gives the instrument greater flexibility when studying underlying colour mechanisms and investigating different visual pathologies.

REFERENCES

Foster, D.H. & Snelgar, R.S. (1983). *Vision Res.* **23**, 787–797.
King-Smith, P.E. & Carden, D. (1976). *J. Opt. Soc. Am.* **66**, 709–717.
Kulikowski, J.J. & Walsh, V. (1991). In *Limits of Vision*, ed. Kulikowski, J.J., Walsh, V. & Murray, I.J., pp. 202–220. Macmillan Press, London.

A simplified histological method for visualizing whisker barrels in the SI cortex of the rat in relationship to intracellularly stained neurones

J. Houchin and S. Bartley

Department of Physiology, Queen Mary & Westfield College, Mile End Road, London E1 4NS

Recent studies (Armstrong-James *et al.* 1994) have shown in adult rats that novel innocuous experiences can produce changes in neuronal behaviour within SI neocortex rats consistent with Hebbian theories of experience-dependent potentiation and weakening of synaptic efficacy for correlated and uncorrelated inputs respectively. We are now exploiting *in vivo* intracellular staining techniques (Houchin, 1973) (a) to look for possible structural changes in neurones after 30 days of such experiences and (b) to relate structure to function, and need to know the position of each stained neurone relative to the whisker barrels. It is possible to combine cytochrome oxidase (CO) staining of barrels (Wong-Riley, 1979) with horseradish peroxidase (HRP) processing of injected neurones in the same sections (Ito, 1992). However, we can now visualize barrels in unstained sections, allowing use of other intracellular stains (including Lucifer Yellow and Biocytin, which are compromised by CO staining of barrels and are usually only viewed in alternate sections adjacent to CO-stained sections; see Hübener & Bolz, 1992 and Levitt *et al.* 1994). Our recent work has required CO staining of barrels for location of small lesions marking recording positions. We found that taking care over flattening the cortex enabled visualization of barrels in unstained sections; with minimum aperture on the microscope condenser, the septa between barrels appear as grey rings of nuclei. The unstained section with the clearest barrel-image was consistently the one best stained with CO (the section through the centre of the barrel) and the top and bottom of the barrel were predictable. The best unstained section now allows us, within the same rat strain, to extrapolate the equivalent 'virtual' CO picture without the complications and hazards of the CO staining itself, as well as avoiding the above incompatibility problems.

Method: The rat is deeply anaesthetized with urethane and perfused with 3% formaldehyde in 0·1 M phosphate

buffer solution (PBS). The brain is left in fixative for at least 12 h. Subcortical structures are then removed by blunt dissection, and the left and right cortices clamped side by side between two glass slides with 2·5 mm spacing. They are placed in 200 ml of 20% sucrose made up in 0·1 M PBS which is replaced about 1 day later. The cortex is flattened again during initial freezing (held under four stacked microscope slides) on a Peltier stage held at −20 °C. Serial sections of 50–100 μm are cut on a freezing microtome (blade at about +20 °C) then floated in PBS in multi-well trays. Camera lucida drawings are made from wet sections of the appropriate unstained barrels (viewed with phase contrast optics) together with the corresponding pattern of blood vessels (in a room free of UV light if fluorescent dyes are used). Most blood vessels are parallel to each other (i.e. perpendicular to the cortical surface and the section). This blood vessel framework allows precise placing of the stained neurone and its arborizations relative to the barrel field. Avoiding the CO histochemistry (avoiding the above-mentioned incompatibility problems) allows not only viewing of the whole neurone but also exploitation of other multiple staining techniques, in combination with visualization of barrels; it should also enable use of, e.g., Lucifer Yellow with immunofluorescence to detect specific receptor proteins on injected neurones (see Belichenko & Dahlström, 1994) in specific positions within the barrel field.

Supported by the Wellcome Trust.

REFERENCES

Armstrong-James, M., Diamond, M.E. & Ebner, F.F. (1994). *J. Neurosci.* **14**, 6978–6991.
Belichenko, P.V. & Dahlström, A. (1994). *J. Neurosci. Meth.* **52**, 111–118.
Houchin, J. (1973). *J. Physiol.* **232**, 67–69P.
Hübener, M. & Bolz, J. (1992). *J. Comp. Neurol.* **324**, 67–80.
Ito, M. (1992). *J. Physiol.* **454**, 247–265.
Levitt, J.B., Yoshioka, T. & Lund, J.S. (1994). *J. Comp. Neurol.* **342**, 551–570.
Wong-Riley, M. (1979). *Brain Res.* **171**, 11–28.

Velocity distribution in non-planar curved phantom measured by MRI

Q. Long*, D.J. Doorly*, M. Tarnawski*, K.T. Scott*, C.L. Dumoulin† and C.G. Caro*

**Centre for Biological and Medical Systems, Imperial College, London SW7 2BX and †GE R & D Center, Schenectady, NY, USA*

Contrary to current belief, arterial curvature and branching commonly appear to be non-planar and associated with non-planar-type flow. To increase understanding, we measured steady flow in a circular tube phantom comprising two successive planar bends (75 deg arc, radii/radii of curvature 0·1) arranged approximately orthogonally. Flow entering the first bend was laminar and fully developed. Using a 1·5 Tesla MR scanner (GE Medical Systems) we measured axial velocity at seven stations along the phantom (Fig. 1) by a 3-D phase contrast sequence (slices 0·3 cm thick, orthogonal to tube axis, spatial resolution 0·04 cm). Marker tubes established phantom orientation.

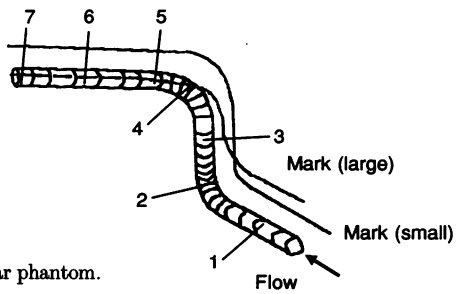

Fig. 1. Non-planar phantom.

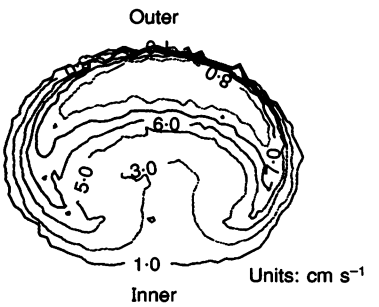

Fig. 2. Axial velocity contour image, stn. 2.

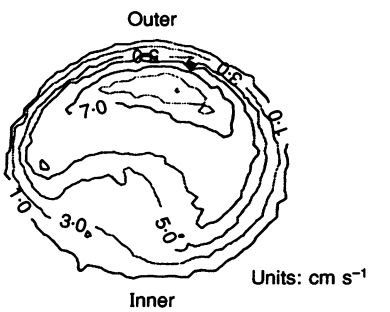

Fig. 3. Axial velocity contour image, stn. 4.

Experiments were performed at Reynolds numbers of 850 (reported results) and 1200; tube cross-sections in bends were slightly elliptical. At first bend (stn. 2) velocity distribution was skewed symmetrically about the plane of curvature, with high velocities at outer wall of curvature and low velocities at inner wall of curvature (Fig. 2). At second bend (stn. 4) velocity distribution was skewed asymmetrically and rotated (Fig. 3). Near-wall velocity gradient is expected to be circumferentially more uniform with non-planar than planar curvature (Caro *et al.* 1994). Velocity distributions at first and second bends support that expectation. Non-planarity has implications for arterial biology and disease.

We thank St Mary's NHS Trust.

REFERENCE

Caro, C.G., Doorly, D.J., Tarnawski, M., Scott, K.T., Johnson, M.M. & Dumoulin, C.L. (1994). *J. Physiol.* **475.P**, 60P.